



This is a repository copy of *Stable steady-state solutions of some biological aggregation models*.

White Rose Research Online URL for this paper:  
<https://eprints.whiterose.ac.uk/172467/>

Version: Accepted Version

---

**Article:**

Potts, J. [orcid.org/0000-0002-8564-2904](https://orcid.org/0000-0002-8564-2904) and Painter, K.J. (2021) Stable steady-state solutions of some biological aggregation models. *SIAM Journal on Applied Mathematics*, 81 (3). pp. 1248-1263. ISSN 0036-1399

<https://doi.org/10.1137/20M1348066>

---

© 2021, Society for Industrial and Applied Mathematics. This is an author-produced version of a paper subsequently published in *SIAM Journal on Applied Mathematics*. Uploaded in accordance with the publisher's self-archiving policy.

**Reuse**

Items deposited in White Rose Research Online are protected by copyright, with all rights reserved unless indicated otherwise. They may be downloaded and/or printed for private study, or other acts as permitted by national copyright laws. The publisher or other rights holders may allow further reproduction and re-use of the full text version. This is indicated by the licence information on the White Rose Research Online record for the item.

**Takedown**

If you consider content in White Rose Research Online to be in breach of UK law, please notify us by emailing [eprints@whiterose.ac.uk](mailto:eprints@whiterose.ac.uk) including the URL of the record and the reason for the withdrawal request.



[eprints@whiterose.ac.uk](mailto:eprints@whiterose.ac.uk)  
<https://eprints.whiterose.ac.uk/>

1       **STABLE STEADY-STATE SOLUTIONS OF SOME BIOLOGICAL**  
2       **AGGREGATION MODELS\***

3                   JONATHAN R. POTTS<sup>†</sup> AND KEVIN J. PAINTER<sup>‡</sup>

4       **Abstract.** Aggregation phenomena occur across the biological sciences, from cell adhesion to  
5 insect swarms, animal home ranges to human cities. Understanding the mechanisms by which they  
6 may spontaneously emerge has therefore generated much interest from applied mathematicians. Partial  
7 differential equations (PDEs) with non-local advection offer a popular formalism for studying  
8 aggregations. However, the inherent non-locality, often necessary for ensuring continuum models  
9 are well-posed, makes their study technically challenging. Here, we take a different approach, by  
10 studying a discrete-space system that can be formally related to classical non-local PDE approaches  
11 via a limiting procedure. We show how to find expressions for the asymptotically-stable steady-  
12 states of this discrete-space system, via an energy functional approach. This allows us to predict  
13 the size of aggregations as a function of the underlying movement mechanisms of individual organ-  
14 isms. We apply this to a recent model of cell adhesion, revealing a hysteresis property whereby  
15 the existing aggregations may persist even as the adhesion tendency decreases past the bifurcation  
16 point. We compare this to numerical solutions of the associated non-local PDE system, showing that  
17 the hysteresis property predicted by the discrete-space expressions is also present in the continuum  
18 system.

19       **Key words.** Aggregation equation, bifurcation, cell adhesion, hysteresis, non-local taxis, partial  
20 differential equation

21       **AMS subject classifications.** 35B32, 35B36, 35B40, 35G20, 35Q92, 92B05

22       **1. Introduction.** Spontaneous aggregations emerge in a wide range of natural  
23 systems. For example, individual animals often aggregate into swarms, herds, schools,  
24 or flocks [30, 20, 35]; cells can aggregate to form various phenomena, such as muscle  
25 tissue, slime mould plasmodia, cancers, and embryos [12, 19, 32]; humans aggregate  
26 in cities and towns [36], and many other animal species group themselves into home  
27 ranges, each confining their movements to a smaller area than their locomotive capa-  
28 bilities allow [7].

29       Mathematical models are key to understanding the mechanisms that give rise to  
30 such aggregated phenomena. Often they take the form of advection-diffusion equa-  
31 tions, with a non-local advection term modelling the movement of individuals in  
32 response to the presence of others [24, 23, 33, 18]. Indeed, equations with non-local  
33 advection are sometimes termed ‘aggregation-diffusion equations’ to emphasise the key  
34 emergent phenomenon they capture [13]. However, not all the non-local advection-  
35 diffusion equations that have been used to model biological aggregations fit neatly  
36 into the usual definition of an aggregation-diffusion equation [11].

37       The popularity of non-local advection-diffusion equations is in part due to their  
38 successful usage in answering a broad range of biological questions. For example,  
39 [3] used such equations to understand cell sorting behaviours, whereby homogeneous  
40 mixtures of two different cell types spontaneously separate into specific arrangements.  
41 They showed that this behaviour can be explained by a process of cell-cell adhesion,  
42 thus verifying mechanistic hypotheses behind observed spatial patterns. To give an ex-

---

\*Submitted to the editors on 24th June 2020.

<sup>†</sup>School of Mathematics and Statistics, University of Sheffield, Hicks Building, Hounsfield Road, Sheffield, S3 7RH, UK ([j.potts@sheffield.ac.uk](mailto:j.potts@sheffield.ac.uk), <http://jonathan-potts.staff.shef.ac.uk/>).

<sup>‡</sup>Dipartimento Interateneo di Scienze, Progetto e Politiche del Territorio (DIST), Viale Pier Andrea Mattioli, 39, 10125 Torino, Italy. ([kevin.painter@polito.it](mailto:kevin.painter@polito.it), <http://www.macs.hw.ac.uk/~painter/>).

43 ample from animal ecology, [4] showed how locust swarms, consisting of one grouping  
44 on the ground and another separate collective in the air, can emerge from long-range  
45 (non-local) attraction and short-range repulsion. Non-local advection-diffusion equa-  
46 tions were also used by [8] to show how wolves form home ranges, in the absence  
47 of conspecifics, from non-local attraction to their own scent markings. Models for  
48 human pedestrian flow have also been proposed using a non-local advection-diffusion  
49 formalism [16].

50 Given the broad applicability of non-local advection-diffusion equations, combined  
51 with the non-trivial technical aspects of dealing with non-locality, there has been  
52 significant mathematical attention paid to such equations in recent years. These  
53 include classical questions of existence and uniqueness, pattern formation properties,  
54 blow-up, and bifurcations (e.g. [33, 5, 22, 6, 9, 14, 21]). Furthermore, these are  
55 often tied to important physical or biological questions. For good recent reviews see  
56 [13, 15, 11].

57 Despite this proliferation of research attention, to our knowledge the question of  
58 predicting aggregation size, given the underlying adhesion mechanisms, has not yet  
59 been explicitly examined. However, the ability to predict the size of aggregations  
60 from the underlying mechanisms is of clear biological importance. If it were possible  
61 to find exact expressions for steady-state solutions, an answer to this question would  
62 naturally follow, as would other properties such as bifurcation structures and the  
63 existence (or otherwise) of hysteresis. However, this is not a trivial task, given the  
64 technical difficulties inherent in using non-local advection.

65 Here, rather than using the formalism of non-local advection-diffusion equations  
66 directly, we instead search for steady-state solutions in a one-dimensional discrete-  
67 space system of ordinary differential equations (ODEs) that is formally related to a  
68 wide class of non-local advection-diffusion equations. Specifically, the continuum limit  
69 of our discrete-space system is identical to the local limit of the non-local advection  
70 diffusion equations (where the local limit is defined to be the limit as the non-local  
71 averaging becomes arbitrarily narrow). The advantage of our approach is that we  
72 are able to find an exact formulation of the stable steady-states of the system, via  
73 minimising the associated energy (or Lyapunov) functional. This then enables us to  
74 calculate exactly the size of any resulting aggregation, as well as revealing bifurcation  
75 structures and hysteresis properties.

76 To demonstrate our technique, we apply it to a specific model of cell-cell adhesion  
77 introduced in [25]. This model is a non-local advection-diffusion equation, but we focus  
78 first on the associated local discrete-space system. We show how the height and width  
79 of resulting aggregations (in discrete-space) depend on the underlying mechanisms:  
80 the adhesion rate, the population size, and the ‘packing constraint’ (ensuring one  
81 cannot have an arbitrarily large number of cells at a given point). We also reveal  
82 hysteresis in the system, whereby for certain parameters the system has a constant  
83 stable steady-state as well as a stable steady-state where aggregations occur. We use  
84 the resulting solutions to construct a bifurcation diagram which we verify through  
85 numerical bifurcation analysis of the underlying discrete-space system of ODEs.

86 We then demonstrate, via numerical simulations, that the associated non-local  
87 continuum model – the one originally introduced in [25] – also has a similar bifurca-  
88 tion structure. Indeed, as the length scales in the non-local terms are decreased in  
89 size (i.e. towards the local limit), the parameter regime where we observe hysteresis  
90 appears to tend towards that predicted by the discrete-space solutions. This demon-  
91 strates that insights from our discrete-space model can be used to inform properties  
92 of the non-local advection-diffusion equation that may be difficult to ascertain by

93 directly analysing the continuum model. The success of this example suggests that  
 94 our method may be widely applicable in understanding steady-states of non-local  
 95 advection-diffusion equations more generally.

96 The paper is organised as follows. In Section 2 we motivate the problem from the  
 97 perspective of non-local continuous-space models. Section 3 outlines our approach  
 98 to examining biological aggregations using discrete-space systems. Section 4 gives  
 99 detailed analysis of a particular model of cell adhesion in a discrete-space setting.  
 100 Section 5 compares the results in the discrete-space setting with numerics from the  
 101 motivating non-local continuous-space model. Section 6 gives some discussion of the  
 102 results, together with concluding remarks.

103 **2. Motivation from non-local continuous-space models.** Our analysis is  
 104 motivated by two 1D examples of non-local advection-diffusion equations. The first  
 105 is given as follows

$$(2.1) \quad \frac{\partial u}{\partial t} = \frac{\partial^2}{\partial x^2}[D(u)] - \frac{\partial}{\partial x} \left[ \chi(u) \int_{-\infty}^{\infty} \frac{s}{|s|} \Omega_{\xi}(|s|) u(x+s, t) ds \right].$$

106 Here,  $u(x, t)$  is the density of individuals (cells or organisms) at location  $x$  and time  
 107  $t$ ;  $D(u)$  and  $\chi(u)$  are smooth functions. The function  $\Omega_{\xi}(s)$  is defined on  $[0, \infty)$  and  
 108 has a local limit that satisfies

$$(2.2) \quad \lim_{\xi \rightarrow 0} \int_0^{\infty} s^{2n+1} \Omega_{\xi}(s) ds = \begin{cases} \frac{1}{2}, & \text{for } n = 0, \\ 0, & \text{for } n \in \mathbb{Z}_{>0}. \end{cases}$$

109 An example of such a function would be  $\Omega_{\xi}(s) = e^{-s/\xi}/(2\xi^2)$ . Here, attraction  
 110 between organisms is greater when they are closer together and gradually decays as the  
 111 distance between them increases. In this example, interactions extend to an arbitrarily  
 112 large distance between organisms, albeit with strength that decays exponentially. To  
 113 circumvent this, functions that are zero for large  $s$ , such as  $\Omega_{\xi}(s) = 1/\xi^2$  (resp.  
 114  $\Omega_{\xi}(s) = 0$ ) for  $s < \xi$  (resp.  $x \geq \xi$ ), are sometimes used instead. Examples of the  
 115 model in Equation (2.1) can be found in, e.g. [24, 25].

116 The second class of non-local advection-diffusion model pertinent to our work is

$$(2.3) \quad \frac{\partial u}{\partial t} = \frac{\partial^2}{\partial x^2}[D(u)] - \frac{\partial}{\partial x} \left[ \chi(u) \frac{\partial}{\partial x} (\mathcal{K}_{\xi} * u) \right].$$

117 Here,  $\mathcal{K}_{\xi}(x)$  is a probability density function, defined on  $\mathbb{R}$  and symmetric about 0,  
 118 such that  $\lim_{\xi \rightarrow 0} \mathcal{K}_{\xi}(x) = \delta(x)$ , the Dirac delta function. For example, one might  
 119 choose  $\mathcal{K}_{\xi}(x) = e^{-|x|/\xi}/(2\xi)$ . Also,  $\mathcal{K}_{\xi} * u$  is the following convolution

$$(2.4) \quad (\mathcal{K}_{\xi} * u)(x) = \int_{-\infty}^{\infty} \mathcal{K}_{\xi}(y-x) u(y) dy.$$

120 Examples of the model in Equation (2.3) can be found in, e.g. [33, 10, 31].

121 Equation (2.1) can often be written in the form of Equation (2.3) [11]. This is  
 122 possible when one can construct a function  $\mathcal{K}_{\xi}(x)$ , symmetric about the origin, such  
 123 that  $\mathcal{K}'_{\xi}(x) = \Omega_{\xi}(x)$  for  $x > 0$ , and  $\lim_{x \rightarrow \pm\infty} \mathcal{K}_{\xi}(x) = 0$  (details in Appendix A of  
 124 [11]). However, here we separate Equations (2.1) and (2.3) out, as the two forms each  
 125 appear in slightly different parts of the literature.

126 The characteristic width,  $\xi$ , of the non-local kernels,  $\Omega_{\xi}$  and  $\mathcal{K}_{\xi}$ , will clearly have  
 127 an effect on the size of the aggregation that emerges. Consequently it is valuable to

128 examine the limit as  $\xi \rightarrow 0$ . For both models (Equations (2.1) and (2.3)), this limit  
 129 leads to the following equation

$$(2.5) \quad \frac{\partial u}{\partial t} = \frac{\partial^2}{\partial x^2} [D(u) - \phi(u)],$$

130 where  $\phi'(u) = \chi(u)$ .

131 The trouble with analysing Equation (2.5) directly is that it can be unstable  
 132 to perturbations at arbitrarily high wavenumbers, i.e. the linear pattern formation  
 133 problem is ill-posed. To see this, let  $U$  be the population size and suppose we are  
 134 working on the interval  $[0, L]$ . Let  $\bar{u} = u - U/L$  and look for solutions of the form  
 135  $\bar{u} = u_0 \exp(\sigma t + i\kappa x)$  valid at short times. Then, by neglecting non-linear terms,  
 136 Equation (2.5) becomes

$$(2.6) \quad \sigma \bar{u} = \kappa^2 [\chi(U/L) - D'(U/L)] \bar{u}.$$

137 Thus, if  $\chi(U/L) > D'(U/L)$  then  $\sigma$  is an increasing (quadratic) function of  $\kappa$ , so  
 138 the linear stability problem is ill-posed: Equation (2.5) is unstable to perturbations  
 139 at arbitrarily high wavenumbers. Conversely, if  $\chi(U/L) \leq D'(U/L)$  then  $\sigma$  is non-  
 140 positive for all values of  $\kappa$ , so patterns cannot form from small perturbations of the  
 141 constant steady-state solution.

142 To circumvent this problem, we instead study a discrete-space model that, being  
 143 a system of ordinary differential equations, has a unique classical solution for any  
 144 appropriate initial condition. We will then show that this model has a continuum  
 145 limit that generalises Equation (2.5).

146 **3. A general discrete-space approach.** We define our discrete-space model  
 147 on a one-dimensional lattice with  $N+1$  sites,  $i \in \{0, \dots, N\}$ , and lattice spacing  $l$ . Let  
 148  $U_i(t)$  be the number of individuals at site  $i$  and time  $t$ . The movement of individuals  
 149 is governed by the following equations

$$(3.1) \quad \begin{aligned} \frac{dU_0}{dt} &= \lambda [T_d(U_1) - T_d(U_0)], \\ \frac{dU_i}{dt} &= \lambda [T_d(U_{i-1}) - 2T_d(U_i) + T_d(U_{i+1})], \quad \text{for } i \in \{1, \dots, N-1\}, \\ \frac{dU_N}{dt} &= \lambda [T_d(U_{N-1}) - T_d(U_N)], \end{aligned}$$

150 where  $T_d(U_i)$  is a non-constant, analytic function and  $\lambda$  is the jump-rate between  
 151 adjacent sites. In principle,  $T_d(U_i)$  can be arbitrary, but in Section 4 we examine a  
 152 specific functional form relevant to biological aggregations. Taking the limit as

$$(3.2) \quad \lambda, N, i \rightarrow \infty; l \rightarrow 0; l^2 \lambda \rightarrow d; il \rightarrow x; lN \rightarrow L$$

153 where  $d, x, L \in \mathbb{R}_{>0}$  leads to the following partial differential equation (Appendix A)

$$(3.3) \quad \frac{\partial u}{\partial t} = d \frac{\partial^2}{\partial x^2} [T_c(u)],$$

154 defined on  $[0, L]$  with zero-flux boundary conditions, where  $u(x, t) = \lim[U_{\lfloor x/l \rfloor}(t)/l]$  is  
 155 the density of individuals at location  $x$  and time  $t$ , and  $T_c[u(x, t)] = \lim T_d[U_{\lfloor x/l \rfloor}(t)]/l$ .

156 Notice that, if  $T_c(u) = [D(u) - \phi(u)]/d$ , Equation (3.3) is exactly the same as  
 157 Equation (2.5). This formalises the relationship between the discrete-space models

158 studied in this section (System 3.1) and the non-local continuum models discussed in  
 159 Section 2 (Equations (2.1) and (2.3)), the latter of which are prevalent in the literature  
 160 [1, 24, 3, 33, 25, 10].

161 A direct calculation reveals that Equation (3.1) conserves mass, i.e.

$$(3.4) \quad \frac{d}{dt} \sum_{i=0}^N U_i = 0,$$

162 so let  $P_d$  be the total size of the population. Another direct calculation shows that  
 163 steady-states of Equation (3.1) occur whenever there is some constant  $\mu$  such that

$$(3.5) \quad T_d(U_i) = \mu$$

164 for all  $i \in \{0, \dots, N\}$ . An example of this situation is given in Figure 1.

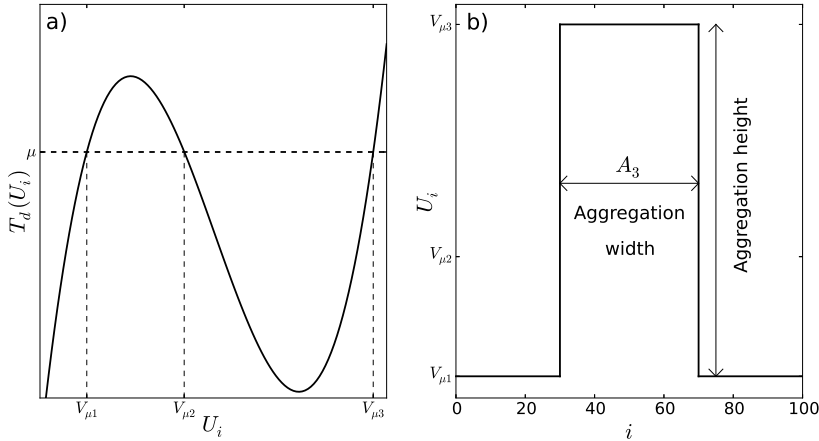


FIG. 1. **Graphical explanation of notation.** Panel (a) shows an example function for  $T_d(U_i)$ . Steady-states of System (3.1) occur whenever there is some constant  $\mu$  such that  $T_d(U_i) = \mu$  for all  $i \in \{0, \dots, N\}$  (Equation 3.5). In the example shown, there are three possible values that  $U_i$  can take for the particular given value of  $\mu$ . These are denoted by  $V_{\mu 1}, V_{\mu 2}, V_{\mu 3}$ . Panel (b) illustrates one possible corresponding steady-state solution. We denote by  $A_j$  the number of integers  $i$  for which  $U_i = V_{\mu j}$  ( $j = 1, 2, 3$ ). In this example,  $A_1 = 60, A_2 = 0$ , and  $A_3 = 41$  (only  $A_3$  is shown on the graph, for simplicity). Note that, by construction,  $A_1 + A_2 + A_3 = N + 1$  where  $N + 1$  is the number of lattice sites, and  $A_1 V_{\mu 1} + A_2 V_{\mu 2} + A_3 V_{\mu 3} = P_d$ , where  $P_d$  is the total population size (see Equations 3.9 and 3.10). This constrains the set of possible steady-state solutions associated to each  $\mu$ . Note also that no value of  $U_i$  can be greater than  $P_d$  (or less than 0) for any  $i$ , so values of  $\mu$  for which the roots of  $T_d(U_i) = \mu$  are all greater than  $P_d$  (or less than 0) cannot lead to steady-state solutions to System 3.1.

165 The first task in understanding the formation of aggregations is to examine when  
 166 the constant steady-state,  $U^* = P_d/(N + 1)$ , is unstable to linear perturbations (here  
 167 the superscript asterisk is used to denote steady-state, and recall that  $P_d$  is the total  
 168 population size). In such cases, small spatially non-constant perturbations grow in  
 169 time and may end up forming aggregations spontaneously. To this end, let  $\bar{U}_i =$   
 170  $U_i - U^*$  and  $\mathbf{W} = (\bar{U}_0, \dots, \bar{U}_N)^T$ . Then, after neglecting non-linear terms, we arrive

171 at the following matrix equation

$$(3.6) \quad \frac{d\mathbf{W}}{dt} = \lambda T'_d(U^*) A \mathbf{W},$$

$$A = \begin{pmatrix} -1 & 1 & 0 & \dots & 0 & 0 & 0 \\ 1 & -2 & 1 & \dots & 0 & 0 & 0 \\ 0 & 1 & -2 & \dots & 0 & 0 & 0 \\ \vdots & \vdots & \vdots & \ddots & \vdots & \vdots & \vdots \\ 0 & 0 & 0 & \dots & -2 & 1 & 0 \\ 0 & 0 & 0 & \dots & 1 & -2 & 1 \\ 0 & 0 & 0 & \dots & 0 & 1 & -1 \end{pmatrix}.$$

172 It was shown in [2] that the eigenvalues of  $A$  all lie in  $(-4, 0]$ . In particular, they are  
 173 non-positive, so for the eigenvalues of the matrix  $T'_d(U^*)A$  to be positive, we require  
 174 the value of  $T'_d(U^*)$  to be negative. In this case the constant steady state is linearly  
 175 unstable at all eigenvalues, suggesting that in the  $T'_d(U^*) < 0$  region patterns will  
 176 form spontaneously.

177 It may also be possible for patterns to form due to the effect of non-linear terms  
 178 outside the region of linear instability. To determine whether this is the case, we find  
 179 non-constant stable steady-states of the system by using an energy (or Lyapunov)  
 180 functional approach. The energy functional for Equation (3.1) has the following form

$$(3.7) \quad E_d[U_0(t), \dots, U_N(t)] = \sum_{i=0}^N F_d(U_i),$$

181 where  $F'_d(U_i) = T_d(U_i)$ . The following calculation shows that  $E_d$  can never increase  
 182 over time

$$(3.8) \quad \begin{aligned} \frac{dE_d}{dt} &= \sum_{i=0}^N \frac{dU_i}{dt} T_d(U_i) \\ &= \lambda T_d(U_0)[T_d(U_1) - T_d(U_0)] + \lambda T_d(U_N)[T_d(U_{N-1}) - T_d(U_N)] \\ &\quad + \lambda \sum_{i=1}^N [T_d(U_{i-1}) - 2T_d(U_i) + T_d(U_{i+1})] T_d(U_i) \\ &= -\lambda \sum_{i=1}^N [T_d(U_i) - T_d(U_{i-1})]^2 \leq 0. \end{aligned}$$

183 Provided Equation (3.7) is bounded below (which we show later), System (3.1) will  
 184 thus tend towards a local minimum of Equation (3.7). This local minimum occurs  
 185 when the derivative of  $E_d$  is zero, which coincides with the values of  $U_i$  where Equation  
 186 (3.5) is satisfied. Thus, finding the stable steady-states of System (3.1) requires us to  
 187 find local minima of Equation (3.7) that also satisfy Equation (3.5).

188 It is possible to find these local minima via a search through a finite range of  
 189 possibilities, as follows. For each  $\mu$  (from Equation 3.5), let  $\{V_{\mu 1}, \dots, V_{\mu M_\mu}\}$  be  
 190 the real-valued solutions to Equation (3.5) such that  $0 \leq V_{\mu j} \leq P_d$  (see Figure  
 191 1). (Here,  $M_\mu$  is the number of real-valued solutions to Equation (3.5).) Finding  
 192 the local minima of Equation (3.7), requires searching through all possible  $\mu$  and



193  $A_1, \dots, A_{M_\mu} \in \{0, \dots, N\}$  such that

$$(3.9) \quad P_d = \sum_{j=1}^{M_\mu} A_j V_{\mu j},$$

$$(3.10) \quad N + 1 = \sum_{j=1}^{M_\mu} A_j.$$

194 Since  $V_{\mu j}$  must be both non-negative and less than or equal to  $P_d$ , for all  $j$ , we need  
 195 only search through  $\mu \in [\mu_{\min}, \mu_{\max}]$  where  $\mu_{\min} = \min_{U_i} \{T_d(U_i) | 0 \leq U_i \leq P_d\}$  and  
 196  $\mu_{\max} = \max_{U_i} \{T_d(U_i) | 0 \leq U_i \leq P_d\}$ . Thus we have restricted our search for minimum  
 197 energy solutions to a finite range of values for  $\mu$  and  $A_1, \dots, A_{M_\mu}$ . This both eases  
 198 the computational requirement for finding minimum energy solutions and shows that  
 199 the energy functional (Equation 3.7) is bounded, so tends to a local minimum. In  
 200 the next section, we will demonstrate this search using a specific functional form of  
 201  $T_d(U_i)$  relevant to contact attraction models of collective cell movement. These are  
 202 models of cell movement whereby contact between cells causes mutual attraction.

203 **4. Analysis of a discrete-space contact-attraction model.** Here, we apply  
 204 the technique detailed in Section 3 to a specific model of cell aggregations. The model  
 205 is in the form of Equation (3.1) with

$$(4.1) \quad T_d(U_i) = U_i - \phi(U_i), \quad \phi(U_i) = \frac{RU_i^2}{6}(3K - 2U_i),$$

206 where  $R > 0$  and  $K > 0$  are constants. The motivation for studying this particular  
 207 formalism is that it is related to a model of cell aggregations from a contact-attraction  
 208 process introduced in [25]. This relationship is detailed in Appendix B.

209 We begin by stating a criterion for the constant steady-state,  $U_i = P_d/(N +$   
 210  $1)$ , being unstable to small perturbations. Equation (3.6) and the subsequent text  
 211 gives the general criterion  $T'_d(P_d/(N + 1)) < 0$ , which, for our specific choice of  $T_d$ ,  
 212 rearranges to give the following

$$(4.2) \quad \frac{KR - \sqrt{K^2R^2 - 4R}}{2R} < \frac{P_d}{N + 1} < \frac{KR + \sqrt{K^2R^2 - 4R}}{2R} \quad \text{and} \quad K^2R > 4.$$

213 Next, we use the energy method from Section 3 to search for the global steady-  
 214 state solution to Equations (3.1) and (4.1). Although this method can be used to  
 215 find any local minimum, we restrict our search to the global minimum, for sim-  
 216 plicity. In Equation (4.1),  $T_d(U_i)$  is a cubic. Therefore, for each  $\mu \in \mathbb{R}$ , there  
 217 are at most three real-valued solutions to  $T_d(U_i) = \mu$  for  $\mu \in [\mu_{\min}, \mu_{\max}]$  and at  
 218 least one. Let  $V_{\mu 1}, V_{\mu 2}, V_{\mu 3}$  denote these three solutions, if all three exist (so that  
 219  $T_d(V_{\mu 1}) = T_d(V_{\mu 2}) = T_d(V_{\mu 3}) = \mu$ ). If there are only two distinct real-valued solu-  
 220 tions, denote them by  $V_{\mu 1}, V_{\mu 2}$  and set  $V_{\mu 3} = V_{\mu 2}$ . If there is only one real-valued  
 221 solution, denote it by  $V_{\mu 1}$  and set  $V_{\mu 3} = V_{\mu 2} = V_{\mu 1}$ . Denote by  $A_1 \in \{0, \dots, N\}$  (resp.  
 222  $A_2, A_3$ ) the number of sites that contain  $V_{\mu 1}$  (resp.  $V_{\mu 2}, V_{\mu 3}$ ) individuals, setting  
 223  $A_3 = 0$  if  $V_{\mu 3} = V_{\mu 2}$  and  $A_2 = 0$  if  $V_{\mu 2} = V_{\mu 1}$ .

224 If there are only two real-valued solutions to  $T_d(U_i) = \mu$  then, by Equation (3.10),  
 225  $A_2 = N + 1 - A_1$ . If there are three real-valued solutions then, by Equations (3.9-3.10),



226 we have

$$(4.3) \quad A_2 = \frac{P_d + A_2(V_{\mu 3} - V_{\mu 1}) - V_{\mu 3}(N + 1)}{V_{\mu 2} - V_{\mu 3}},$$

$$(4.4) \quad A_3 = N + 1 - A_2 - A_1.$$

227 Consequently, to find the minimum energy solutions, we need only search through  
 228 values of  $\mu \in [\mu_{\min}, \mu_{\max}]$  and  $A_1 \in \{0, \dots, N\}$ . Then  $A_2$  and  $A_3$  are determined  
 229 by Equations (4.3) and (4.4) respectively, whilst  $V_{\mu 1}, V_{\mu 2}, V_{\mu 3}$  are given by Equation  
 230 (3.5).

231 Due to the constraints on  $A_1, A_2, A_3$  (Equation 4.3, 4.4) and the fact that they  
 232 all have to be elements of  $\{0, \dots, N\}$ , the magnitude of  $N$  may have an effect on the  
 233 existence of a non-constant minimum-energy solution. In reality, organisms will be  
 234 able to move continuously in space, not being constrained by a lattice. Therefore it  
 235 is valuable to search for minimum energy solutions in the large- $N$  limit. Specifically,  
 236 we take the limit given in (3.2), additionally with  $\mu \rightarrow 0$  such that  $\mu/l \rightarrow m$  with  
 237  $0 < m < \infty$ . This latter limit is required to find a solution to  $T_c[u(x, t)] = m$  that  
 238 corresponds to the continuum limit of  $T_d(U_i) = \mu$ , where  $T_c[u(x, t)] = \lim[T_d(U_i)/l]$   
 239 (Appendix A).

240 In this limit,  $T_c(u) = u - ru^2(3k - 2u)/6$  and  $x \in [0, L]$  (Appendix B, Equation  
 241 (B.2)). To reduce parameters, we non-dimensionalise, using the following substitu-  
 242 tions

$$(4.5) \quad \begin{aligned} \tilde{x} &= \frac{x}{L}, \quad \tilde{t} = \frac{tD}{L^2}, \quad \tilde{u}(\tilde{x}, \tilde{t}) = \frac{u(x, t)}{k}, \quad \tilde{r} = rk^2, \\ \tilde{a}_j &= \frac{a_j}{L}, \quad \tilde{T}_c(\tilde{u}) = \frac{T_c(u)}{k}, \quad P = \frac{P_d L}{k}, \quad \tilde{m} = \frac{m}{k}. \end{aligned}$$

243 We henceforth drop the tildes for notational convenience. Then suppose there are  
 244 three distinct, real solutions to  $T_c(u) = m$  and denote them by  $v_{m1}, v_{m2}, v_{m3}$ . We  
 245 arrive at the following expressions

$$(4.6) \quad T_c(u) = u - \frac{ru^2}{6}(3 - 2u),$$

$$(4.7) \quad a_2 = \frac{P + a_1(v_{m3} - v_{m1}) - v_{m3}}{v_{m2} - v_{m3}},$$

$$(4.8) \quad a_3 = 1 - a_1 - a_2,$$

$$(4.9) \quad \mathcal{E}_c(m, a_1) = \sum_{j=1}^3 a_j \left[ \frac{v_{mj}^2}{2} - \frac{rv_{mj}^3}{6} + \frac{rv_{mj}^4}{12} \right].$$

246 Here,  $\mathcal{E}_c(m, a_1)$  is the energy, expressed as a function of  $m$  and  $a_1$ . If there are only  
 247 two distinct real-valued solutions to  $T_c(u) = m$  then denote them by  $v_{m1}$  and  $v_{m2}$ ;  
 248 then set  $v_{m3} = v_{m2}$ ,  $a_2 = 1 - a_1$ , and  $a_3 = 0$ . If there is only one distinct real-valued  
 249 solution to  $T_c(u) = m$  then denote it by  $v_{m1}$ ; then set  $v_{m3} = v_{m2} = v_{m1}$ ,  $a_1 = 1$ ,  
 250  $a_2 = 0$ , and  $a_3 = 0$ . Finding the global steady-state solution requires finding the  
 251 minimum of  $\mathcal{E}_c(m, a_1)$  across all values of  $m \in [m_{\min}, m_{\max}]$  and  $a_1 \in [0, 1]$  such that  
 252  $a_2, a_3 \in [0, 1]$  and  $v_{m1}, v_{m2}, v_{m3} \geq 0$ , where  $m_{\min} = \min_u \{T_c(u) | 0 \leq u \leq P\}$  and  
 253  $m_{\max} = \max_u \{T_c(u) | 0 \leq u \leq P\}$ .

254 The resulting large- $N$  limit of the global minimum energy solution to Equation

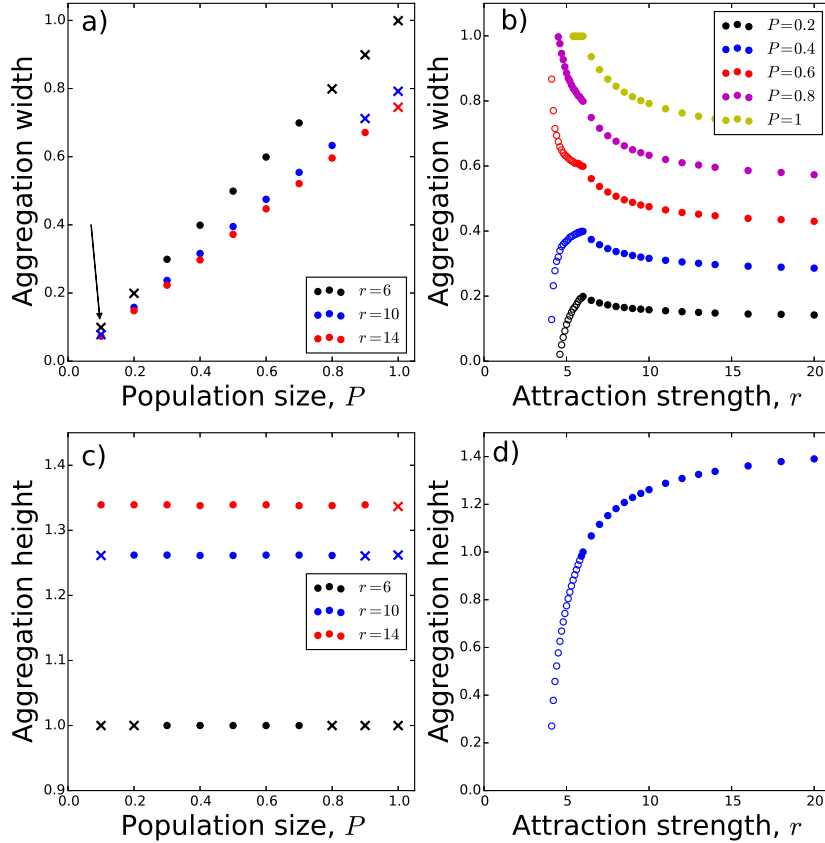


FIG. 2. **Predicted aggregation width.** Panel (a) shows the effect of the population size,  $P$ , on the aggregation width. Dots (resp. crosses) denote situations where the constant steady-state is unstable (resp. stable) to linear perturbations. Note that, in some cases (e.g.  $P = 0.1, r = 6$ , see arrow in Panel a), the constant steady-state is stable, yet the global minimum energy solution is an aggregation. This indicates a hysteresis in the system, whereby aggregations will remain if already formed, but not arise spontaneously from small perturbations of the spatially constant solution. In Panel (b), we see how the aggregation width varies with the strength of contact attraction,  $r$ . The solid dots denote ‘pure’ aggregations whereby only one of  $v_{m_*1}, v_{m_*2}, v_{m_*3}$  (defined in Equation 4.10) is greater than zero. The unfilled circles represent situations whereby more than one of  $v_{m_*1}, v_{m_*2}, v_{m_*3}$  is greater than zero. Panel (c) shows that  $P$  appears not to affect the aggregation height (defined as  $\max_j \{v_{m_*j}\} - \min_j \{v_{m_*j}\}$ ). Panel (d) shows the effect of  $r$  on aggregation height.

255 (3.1), which we denote by  $u_*(x)$ , has the following functional form

$$(4.10) \quad u_*(x) = \begin{cases} v_{m_*1}, & \text{on a subset } S_1 \subseteq [0, 1] \text{ of measure } a_1, \\ v_{m_*2}, & \text{on a subset } S_2 \subseteq [0, 1] \text{ of measure } a_2, \\ v_{m_*3}, & \text{on a subset } S_3 \subseteq [0, 1] \text{ of measure } a_3, \end{cases}$$

256 for some  $m_*$ , using the definitions of  $v_{m_j}$  and  $a_j$  ( $i \in \{1, 2, 3\}$ ) from the previous

257 paragraph. Here,  $S_1, S_2, S_3$  are pairwise disjoint and  $u_*(x)$  is the continuum limit of  
 258 the minimum energy solution for the discrete system (Equation 3.1), with  $T_d(U_i)$  as  
 259 defined in Equation (4.1).

260 To understand the properties of  $u_*(x)$ , we calculate it for a range of parameter  
 261 values,  $r$  and  $P$ . Without loss of generality, suppose that  $v_{m_*1} \geq v_{m_*2} \geq v_{m_*3}$ . Then  
 262 we define  $a_1$  as the *aggregation width* and  $v_{m_*1} - v_{m_*3}$  as the *aggregation height* (see  
 263 Figure 1). (Note that our terminology in calling  $a_1$  the ‘aggregation width’ is merely  
 264 a heuristic nomenclature, based on the case where the set  $S_1$  is connected. However,  
 265 there is no *a priori* reason that  $S_1$  must be connected.)

266 Figure 2 shows the aggregation width and height for the global minimum energy  
 267 solution for various values of  $r$  and  $P$ . For sufficiently large  $r$ , it turns out that  $v_{m_*2}$   
 268 and  $v_{m_*3}$  are (numerically) equal to zero. We call this case a *pure aggregation*. These  
 269 occur for  $r \gtrsim 6$  when  $P = 0.2, 0.4, 0.6$  and for all values of  $r$  we examined when  
 270  $P = 0.8, 1$ . For situations where more than one of  $v_{m_*1}, v_{m_*2}, v_{m_*3}$  are greater than  
 271 zero, it is possible for the whole terrain to have non-zero population density, but have  
 272 some regions of space where the population density is higher than others.

273 It is interesting to examine the parameter values for which the constant steady-  
 274 state is unstable to linear perturbations, and compare this to the set of values where  
 275 the minimum energy solution is non-constant. The large- $N$  limit, dimensionless ver-  
 276 sion of the instability criterion in Equation (4.2) is that  $r > 4$  and  $1 - \sqrt{1 - 4/r} <$   
 277  $2P < 1 + \sqrt{1 - 4/r}$ . For some parameter values, the constant steady-state is stable,  
 278 yet the global minimum energy solution is one where there is an aggregation of  
 279 length less than 1 (see Figure 2a). This indicates a hysteresis in the system, whereby  
 280 aggregations will persist if present, but will not form spontaneously from a small  
 281 non-constant perturbation of the constant steady-state.

282 To understand this hysteresis better, we construct a bifurcation diagram (Figure  
 283 3) for the case  $P = 0.1$ . The top branch gives the aggregation height constructed  
 284 from the minimum energy solutions. The bottom branch corresponds to the results  
 285 of linear stability analysis. We then tested the predictions from Equation (4.10)  
 286 against numerical solutions of the discrete-space system (Equation 3.1) by performing  
 287 a numerical bifurcation analysis, following the method from [27].

288 This numerical method begins by setting a start value for the parameter of inter-  
 289 est, which in our case is  $r = 12$ , and solving to numerical steady-state. Then we  
 290 decrease the value of  $r$ , perturb the solution with small random fluctuations, and  
 291 solve again to numerical steady-state. The process of reducing  $r$ , perturbing the solu-  
 292 tion, and solving to steady-state is then repeated until we reach values of  $r$  for which  
 293 the aggregation patterns disappear (see [27] for more details). Figure 3 shows that  
 294 our predictions are in good agreement with the numerical bifurcation analysis, only  
 295 slightly over-estimating the bifurcation point ( $r = 5.0$  in our predictions and  $r \approx 4.8$   
 296 for the numerics).

297 To solve Equation (3.1) numerically, we used a finite difference approximation  
 298 with time-step  $\Delta t = 0.001$  and  $N = 100$ . We defined the point at which numerical  
 299 steady-state is reached to be the first point in time where  $\sum_i |U_i(t + \Delta t) - U_i(t)| <$   
 300  $10^{-8}$ .

301 **5. Numerical comparison with a non-local continuous-space formula-**  
 302 **tion.** We explore whether the discrete model predicts behaviour of the associated  
 303 non-local PDE (Equation 2.1) using numerical bifurcation analysis. The numerical  
 304 method for solving Equation (2.1) is described in detail in [17], where we set  $D(u) = d$ ,

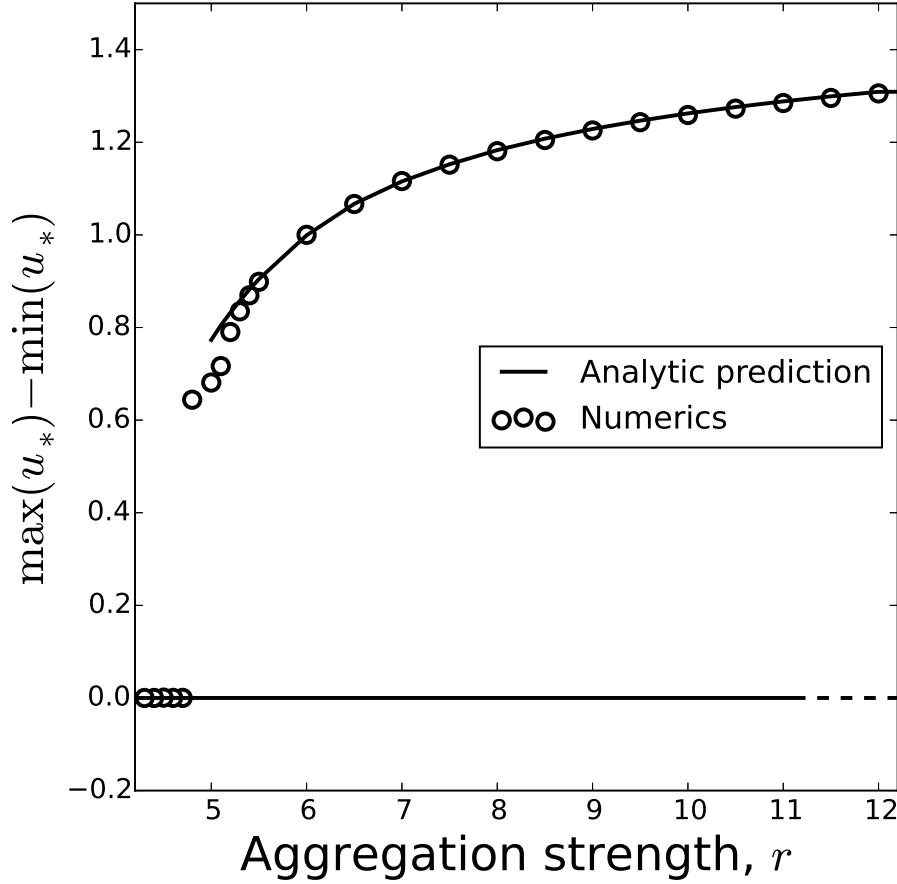


FIG. 3. **Bifurcation diagram.** The solid and dashed lines give predictions from our analysis regarding the steady-states and their stability. Specifically, the top branch is the global minimum energy solution (see Equation (4.10)), where this corresponds to a non-constant solution. The bottom branch gives the stability of the constant steady-state solution: solid if it is stable and dashed if it is unstable. The circles give numerical steady-state solutions from the numerical bifurcation analysis described in the Main Text. Here,  $P = 0.1$ .

305  $\chi(u) = ru(k - u)$ , and the step-form

306 
$$\Omega_\xi(s) = \begin{cases} 1/\xi^2 & s < \xi, \\ 0 & \text{otherwise.} \end{cases}$$

307 These choices lead to (B.3) as  $\xi \rightarrow 0$ , which is the continuum limit of the discrete-space  
 308 model studied in Section 4. As in the discrete model we apply numerical continuation,  
 309 fixing  $P = 0.1$ ,  $k = d = 1$  and treating  $r$  as the bifurcation parameter. Bifurcation  
 310 curves are constructed for various  $\xi$ . Note that decreasing  $\xi$  increases computational  
 311 time due to the finer resolution required for the non-local term, reinforcing the need  
 312 for alternative approaches that do not require numerical solutions, such as those

313 presented here.

314 The uniform steady-state of the non-local aggregation model becomes unstable at  
 315 a critical threshold  $r^*(\xi)$ : this point is straightforward to determine via linear stability  
 316 analysis (see [25]) and, for a finite domain, varies a small amount with  $\xi$ . As would be  
 317 expected, as  $\xi \rightarrow 0$  this converges to the critical value resulting from Equation (2.6).

318 Upper curves in Figure 4(a) describe solution branches corresponding to a (numerically)  
 319 stable single aggregate, with specific solutions illustrated in (b) and (c). Each  
 320 curve is composed from supercritical and subcritical branches that extend about  $r^*(\xi)$ .  
 321 Subcritical extensions indicate a corresponding hysteresis phenomenon to that noted  
 322 for the discrete model. These branches terminate at a lower threshold  $r^{**}(\xi)$ , below  
 323 which the aggregating component is overwhelmed by diffusion. Notably, lowering  $\xi$   
 324 decreases  $r^{**}(\xi)$ , yet each computed value of  $r^{**}(\xi)$  is strictly higher than the corre-  
 325 sponding bifurcation point ( $r = 5.0$ ) predicted by our analysis of the discrete-space  
 326 system (Figure 3). We conjecture that, were it possible to continue the numerical  
 327 analysis of the non-local continuum model to arbitrarily low values of  $\xi$ , the location  
 328 of  $r^{**}(\xi)$  would tend towards  $r = 5.0$ . Unfortunately, moving  $\xi > 0$  considerably  
 329 below 0.01 becomes computationally infeasible inside a reasonable time frame.

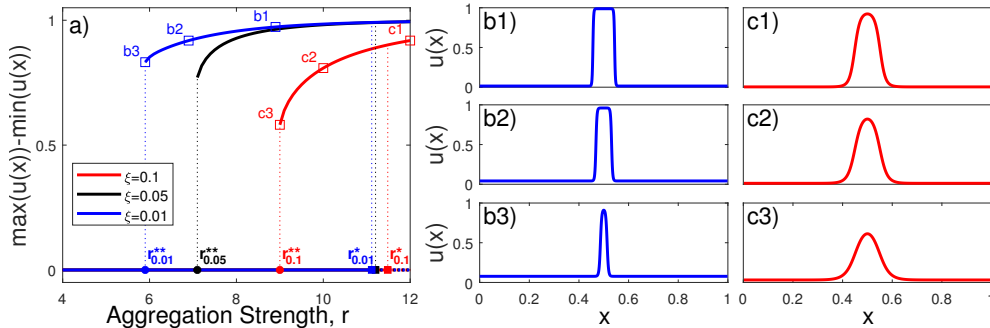


FIG. 4. **Bifurcation diagram for a nonlocal aggregation model.** (a) Solid lines show (numerically) computed stable steady-states under different values of sensing radius  $\xi$ . Specifically, the top branch describes a single cluster with the bottom branch showing the stability of the constant steady-state solution. The bottom branch becomes unstable at the critical threshold  $r_{\xi}^*$ , as predicted via linear stability analysis. The subcritical branch of the single cluster solution remains stable down to some lower threshold  $r_{\xi}^{**}$ , below which the cluster collapses and disperses. Solutions at the points marked by squares are shown in the plots in (b1)-(b3) and (c1)-(c3). For these plots, we set  $P = 0.1$ ,  $d = 1$  and  $k = 1$ .

330 **6. Discussion.** We have shown how to gain understanding into the size and  
 331 hysteresis properties of biological aggregations by using a discrete-space model. This  
 332 model can be formally related to the oft-used aggregation equation formalism, but has  
 333 the advantage of being amenable to exact analysis of the steady-state solutions. We  
 334 tested our resulting equations against a particular model of cell adhesion and showed  
 335 that they are in good agreement with discrete-space numerics (Figure 3). Thus this  
 336 approach provides a quick way of giving quite a detailed description of bifurcation  
 337 structure in discrete-space aggregation models.

338 We also investigated the extent to which these predictions carry over to a corre-  
 339 sponding non-local continuum model that is often used to study aggregation phenom-  
 340 ena (Equation 2.1). This involved numerical simulations of this non-local continuum  
 341 model, which are summarised in Figure 4. We observe some clear similarities between

342 the discrete-space results and the continuum results, but also some clear differences.

343 Notably, guided by the identification of hysteresis in the discrete model, numerical  
 344 investigation was performed on the continuum model and indeed the same phenom-  
 345 enon was found. Furthermore, as the non-local parameter  $\xi$  tends towards zero, the  
 346 point where the subcritical structure collapses ( $r_{\xi}^{**}$  in Figure 4), appears to tend  
 347 towards the corresponding point in the discrete-space case (Figure 3). However, num-  
 348 erics for small  $\xi$  become increasing time-consuming, so it is of considerable value to  
 349 have a quick technique for deriving the expected limit of  $r_{\xi}^{**}$  as  $\xi \rightarrow 0$ .

350 On the other hand, perhaps the biggest discrepancy between the steady-states  
 351 of the non-local PDE and those of the corresponding discrete-space system is in the  
 352 height of the resulting aggregation. We see in Figure 4 that the steady-state solution  
 353 in the continuous case always appears to be bounded by  $u = 0$  and  $u = 1$ . We expect  
 354 that this arises from the fact that  $\chi(u) = ru(k - u)$  vanishes at  $u = 0$  and  $u = 1$   
 355 when  $k = 1$ . However, the discrete-space system, given by Equations (3.1) and (4.1)  
 356 for  $K = 1$ , does give rise to aggregations whose height is greater than 1 (Figure 3).  
 357 We conjecture that this is because the discrete-space system vanishes at  $U_i = 0$  and  
 358  $U_i = 3/2$  but not when  $U_i = 1$ . Note that none of the aggregations in the numerical  
 359 solutions we examined have height greater than  $3/2$  (Figure 3). By extension, this  
 360 means there is also a discrepancy in the aggregation width between the discrete and  
 361 continuous models.

362 The discrete-space model studied here only incorporates the effect of nearest-  
 363 neighbour lattice sites. However, it may be possible to extend our techniques to  
 364 certain cases where each lattice site is affected by sites beyond its nearest neighbour.  
 365 Such an extension would lead to a more general form of the matrix  $A$  in Equation  
 366 (3.6). If this new matrix has eigenvalues with negative real parts then the same  
 367 condition for linear pattern formation would hold as in our work:  $T'_d(U^*) < 0$ . The  
 368 next step, which we expect would be non-trivial in general, would be to determine  
 369 which forms of the matrix  $A$  allow for a decreasing energy functional, to give a similar  
 370 argument to Equation (3.8). This would be an interesting avenue for future work.

371 Although many recent models of biological aggregation use a non-local continuum  
 372 model, discrete-space formalisms are not without precedent. Indeed, until [3], it was  
 373 typical to use a discrete-space formalism to model the specific process of aggregation  
 374 via cell adhesion (see [3] for references). Perhaps the closest model to the one presented  
 375 here is that of [2]. There, the authors analyse a specific discrete-space model for linear  
 376 pattern formation properties and steady-states, but do not examine the stability of  
 377 non-constant steady-states. Likewise, the effect of the functional form of (3.5) on  
 378 steady-state patterns was analysed in [34], but without any stability analysis of non-  
 379 constant steady-states. Here, we build on both studies by providing an energy method  
 380 to categorise the asymptotic stability of such non-constant steady-states. This makes  
 381 use of a construction of discrete-space energy functionals from [28]. Our method is  
 382 framed in a general context (Section 3) that encompasses both the model in [2] and  
 383 the specific model studied here (Section 4).

384 PDE formalisms are often used because they are amenable to large swathes of  
 385 analytic techniques, whereas discrete models often rely on simulation analysis [29]. In  
 386 contrast, here we given an example of a discrete-space approach that is amenable to  
 387 analysis that has not so far been possible with continuum descriptions. The difficulty  
 388 with the continuum approach is the necessity for non-local advection to ensure the  
 389 problem is well-posed. This disappears in the discrete-space description (indeed, the  
 390 lattice size can be thought of as analogous to non-locality). By then showing that the  
 391 steady-states of the discrete system live in a finite set (something that would lead to

392 trivial solutions in the continuum limit), it is possible to search through the possible  
 393 steady-state solutions for the minimum energy. This would not be so easy using an  
 394 energy description of the non-local continuum model, as the search would be through  
 395 an entire function space rather than a finite set of possible values. In conclusion, we  
 396 suggest that mathematical analysis of discrete-space approximations should remain  
 397 a valuable part of the toolkit for anyone studying mathematical models of biological  
 398 aggregations.

399 **Appendix A. Continuum limit of the general model.** Here we show how  
 400 Equation (3.1) leads to Equation (3.3) in the limit as  $\lambda, N, i \rightarrow \infty$  and  $l \rightarrow 0$  such that  
 401  $l^2\lambda \rightarrow d$ ,  $il \rightarrow x$ , and  $lN \rightarrow L$  for  $d, L \in \mathbb{R}_{>0}$ . Using  $\lim$  to denote this limit, we define  
 402  $u(x, t) = \lim[U_{\lfloor x/l \rfloor}(t)/l]$  and  $T_c[u(x, t)] = \lim T_d[U_{\lfloor x/l \rfloor}(t)]/l$ . Then, for  $0 < i < N$ ,  
 403 we have

$$(A.1) \quad \lim \left( \frac{1}{l} \frac{dU_i}{dt} \right) = \lim \left( \frac{d}{dt} \left( \frac{U_{x/l}}{l} \right) \right) = \frac{\partial u}{\partial t},$$

404 and

$$(A.2) \quad \begin{aligned} & \lim \left( \frac{\lambda}{l} [T_d(U_{i-1}) - 2T_d(U_i) + T_d(U_{i+1})] \right) \\ &= \lim \left( \lambda \frac{[T_d(U_{(x-l)/l}) - 2T_d(U_{x/l}) + T_d(U_{(x+l)/l})]}{l} \right) \\ &= \lim \left( \lambda l^2 \frac{[T_d(U_{(x-l)/l})/l - 2T_d(U_{x/l})/l + T_d(U_{(x+l)/l})/l]}{l^2} \right) \\ &= d \frac{\partial^2}{\partial x^2} [T_c(u)]. \end{aligned}$$

405 By Equation (3.1), we can equate Equations (A.1) and (A.2) to give

$$(A.3) \quad \frac{\partial u}{\partial t} = d \frac{\partial^2}{\partial x^2} [T_c(u)],$$

406 which is Equation (3.3).

407 For the boundary conditions, we can take the continuum limit of either the top  
 408 or bottom row of Equation (3.1). We start by looking at the bottom row, which gives  
 409 the zero-flux boundary condition at  $x = L$ . For the left-hand side, we have

$$(A.4) \quad \lim \left( \frac{dU_N}{dt} \right) = \lim \left( l \frac{d}{dt} \left( \frac{U_{L/l}}{l} \right) \right) = 0 \times \frac{\partial u}{\partial t} \Big|_{x=L} = 0.$$

410 For the right-hand side (of the bottom row of Equation (3.1)), we have

$$(A.5) \quad \begin{aligned} & \lim(\lambda[T_d(U_{N-1}) - T_d(U_N)]) \\ &= \lim \left( \lambda l^2 \frac{T_d(U_{(L-l)/l})/l - T_d(U_{L/l})/l}{l} \right) = -d \frac{\partial u}{\partial x} \Big|_{x=L}. \end{aligned}$$

411 Then Equations (A.4) and (A.5) together give the zero flux boundary condition at  
 412  $x = L$ . The calculation of the boundary condition at  $x = 0$  is similar.

413 **Appendix B. Continuum limit of the model in Section 4.** Using the  
 414 notation and limiting procedure from Appendix A, we derive here the continuum



415 limit of Equation (3.1) in the case where

$$(B.1) \quad T_d(U_i) = U_i - \frac{RU_i^2}{6}(3K - 2U_i),$$

416 as defined in Equation (4.1). In addition to the limit from Appendix A, we take the  
417 limit as  $K \rightarrow 0$  and  $R \rightarrow \infty$  such that  $K/l \rightarrow k$  and  $Rl^2 \rightarrow r/d$ . Then

$$(B.2) \quad \begin{aligned} dT_c[u(x, t)] &= \lim[l^2 \lambda T_d(U_i)/l] \\ &= \lim \left[ \frac{l^2 \lambda U_i}{l} - \frac{l^4 \lambda R U_i^2}{6 l^2} \left( \frac{3K}{l} - \frac{2U_i}{l} \right) \right] \\ &= du(x, t) - \frac{ru^2(x, t)}{6}(3k - 2u(x, t)). \end{aligned}$$

418 Hence, by plugging Equation (B.2) into Equation (A.3), the continuum limit of Equa-  
419 tion (3.1) with  $T_d$  as defined in Equation (4.1) is

$$(B.3) \quad \begin{aligned} \frac{\partial u}{\partial t} &= d \frac{\partial^2 u}{\partial x^2} - \frac{\partial^2}{\partial x^2} \left[ \frac{ru^2}{6}(3k - 2u) \right] \\ &= d \frac{\partial^2 u}{\partial x^2} - \frac{\partial}{\partial x} \left[ ru(k - u) \frac{\partial u}{\partial x} \right], \end{aligned}$$

420 which is the local limit (i.e.  $\xi \rightarrow 0$ ) of Equation (2.1) with  $\chi(u) = ru(k - u)$  and  
421  $D(u) = d$ . This functional form for  $\chi(u)$  was studied by [25]. It incorporates a  
422 ‘packing’ constant,  $k$ , accounting for the fact that there is a limit to the amount of  
423 individuals that can be in a given area. Specifically, individuals at  $x$  at time  $t$  will  
424 tend to move up (resp. down) the density gradient when  $0 < u(x, t) < k$  (resp.  
425  $k < u(x, t)$ ). This feature has been shown to be both mathematically important and  
426 biologically realistic in a variety of contexts [26].

427 **Acknowledgements.** This research arose from conversations at the workshop  
428 ‘PDEs in Mathematical Biology: Modelling and Analysis’ at the International Centre  
429 for Mathematics Sciences, Edinburgh, funded by the London Mathematics Society and  
430 Clay Mathematics Institute. We thank all those involved in funding and organising  
431 this workshop. We also thank Thomas Hillen and two anonymous reviewers for helpful  
432 comments on the manuscript.

433

#### REFERENCES

- 434 [1] W. ALT, *Degenerate diffusion equations with drift functionals modelling aggregation*, Nonlinear  
435 Analysis: Theory, Methods & Applications, 9 (1985), pp. 811–836.  
436 [2] K. ANGUIGE AND C. SCHMEISER, *A one-dimensional model of cell diffusion and aggregation,*  
437 *incorporating volume filling and cell-to-cell adhesion*, Journal of Mathematical Biology, 58  
438 (2009), p. 395.  
439 [3] N. J. ARMSTRONG, K. J. PAINTER, AND J. A. SHERRATT, *A continuum approach to modelling*  
440 *cell–cell adhesion*, Journal of Theoretical Biology, 243 (2006), pp. 98–113.  
441 [4] A. J. BERNOFF AND C. M. TOPAZ, *A primer of swarm equilibria*, SIAM Journal on Applied  
442 Dynamical Systems, 10 (2011), pp. 212–250.  
443 [5] A. L. BERTOZZI AND T. LAURENT, *Finite-time blow-up of solutions of an aggregation equation*  
444 *in  $R^n$* , Communications in Mathematical Physics, 274 (2007), pp. 717–735.  
445 [6] A. L. BERTOZZI AND D. SLEPCEV, *Existence and uniqueness of solutions to an aggregation equa-*  
446 *tion with degenerate diffusion*, Communications on Pure and Applied Analysis, 9 (2009),  
447 p. 1617.

- 448 [7] L. BÖRGER, B. D. DALZIEL, AND J. M. FRYXELL, *Are there general mechanisms of animal*  
449 *home range behaviour? a review and prospects for future research*, Ecology Letters, 11  
450 (2008), pp. 637–650.
- 451 [8] B. BRISCOE, M. LEWIS, AND S. PARRISH, *Home range formation in wolves due to scent marking*,  
452 Bull. Math. Biol., 64 (2002), pp. 261–284, <https://doi.org/10.1006/bulm.2001.0273>.
- 453 [9] P.-L. BUONO AND R. EFTIMIE, *Codimension-two bifurcations in animal aggregation models*  
454 *with symmetry*, SIAM Journal on Applied Dynamical Systems, 13 (2014), pp. 1542–1582.
- 455 [10] M. BURGER, M. D. FRANCESCO, S. FAGIOLI, AND A. STEVENS, *Sorting phenomena in a mathe-*  
456 *matical model for two mutually attracting/repelling species*, SIAM Journal on Mathemat-  
457 ical Analysis, 50 (2018), pp. 3210–3250.
- 458 [11] A. BUTTENSCHÖN AND T. HILLEN, *Non-local cell adhesion models: Steady states and bifurca-*  
459 *tions*, arXiv preprint arXiv:2001.00286, (2020).
- 460 [12] M. CABEL, H. J. MEISELMAN, A. S. POPEL, AND P. C. JOHNSON, *Contribution of red blood*  
461 *cell aggregation to venous vascular resistance in skeletal muscle*, American Journal of  
462 Physiology-Heart and Circulatory Physiology, 272 (1997), pp. H1020–H1032.
- 463 [13] J. A. CARRILLO, K. CRAIG, AND Y. YAO, *Aggregation-diffusion equations: dynamics, asymp-*  
464 *totics, and singular limits*, in Active Particles, Volume 2, Springer, 2019, pp. 65–108.
- 465 [14] J. A. CARRILLO, F. JAMES, F. LAGOUTIÈRE, AND N. VAUCHELET, *The filippov characteristic*  
466 *flow for the aggregation equation with mildly singular potentials*, Journal of Differential  
467 Equations, 260 (2016), pp. 304–338.
- 468 [15] L. CHEN, K. J. PAINTER, C. SURULESCU, AND A. ZHIGUN, *Mathematical models for cell migra-*  
469 *tion: a nonlocal perspective*, Philosophical Transactions of the Royal Society of London B,  
470 To appear (2020).
- 471 [16] R. M. COLOMBO, M. GARAVELLO, AND M. LÉCUREUX-MERCIER, *A class of nonlocal models*  
472 *for pedestrian traffic*, Mathematical Models and Methods in Applied Sciences, 22 (2012),  
473 p. 1150023.
- 474 [17] A. GERISCH, *On the approximation and efficient evaluation of integral terms in pde models of*  
475 *cell adhesion*, IMA Journal of Numerical Analysis, 30 (2010), pp. 173–194.
- 476 [18] A. GERISCH AND M. A. CHAPLAIN, *Mathematical modelling of cancer cell invasion of tissue:*  
477 *local and non-local models and the effect of adhesion*, Journal of Theoretical Biology, 250  
478 (2008), pp. 684–704.
- 479 [19] V. V. GLINSKY, G. V. GLINSKY, O. V. GLINSKII, V. H. HUXLEY, J. R. TURK, V. V. MOSSINE,  
480 S. L. DEUTSCHER, K. J. PIENTA, AND T. P. QUINN, *Intravascular metastatic cancer cell*  
481 *homotypic aggregation at the sites of primary attachment to the endothelium*, Cancer  
482 Research, 63 (2003), pp. 3805–3811.
- 483 [20] R. JEANSON, C. RIVAUT, J.-L. DENEUBOURG, S. BLANCO, R. FOURNIER, C. JOST, AND  
484 G. THERAULAZ, *Self-organized aggregation in cockroaches*, Animal Behaviour, 69 (2005),  
485 pp. 169–180.
- 486 [21] G. KAIB, *Stationary states of an aggregation equation with degenerate diffusion and bounded*  
487 *attractive potential*, SIAM Journal on Mathematical Analysis, 49 (2017), pp. 272–296.
- 488 [22] T. LAURENT, *Local and global existence for an aggregation equation*, Communications in Partial  
489 Differential Equations, 32 (2007), pp. 1941–1964.
- 490 [23] C. T. LEE, M. F. HOOPES, J. DIEHL, W. GILLILAND, G. HUXEL, E. V. LEAVER, K. MCCANN,  
491 J. UMBANHOWAR, AND A. MOGILNER, *Non-local concepts and models in biology*, Journal of  
492 Theoretical Biology, 210 (2001), pp. 201–219.
- 493 [24] A. MOGILNER AND L. EDELSTEIN-KESHET, *A non-local model for a swarm*, Journal of Mathe-  
494 matical Biology, 38 (1999), pp. 534–570.
- 495 [25] K. PAINTER, J. BLOOMFIELD, J. SHERRATT, AND A. GERISCH, *A nonlocal model for contact at-*  
496 *traction and repulsion in heterogeneous cell populations*, Bulletin of Mathematical Biology,  
497 77 (2015), pp. 1132–1165.
- 498 [26] K. J. PAINTER AND T. HILLEN, *Volume-filling and quorum-sensing in models for chemosensitive*  
499 *movement*, Can. Appl. Math. Quart, 10 (2002), pp. 501–543.
- 500 [27] K. J. PAINTER AND T. HILLEN, *Spatio-temporal chaos in a chemotaxis model*, Physica D, 240  
501 (2011), pp. 363–375.
- 502 [28] K. J. PAINTER, D. HORSTMANN, AND H. G. OTHMER, *Localization in lattice and continuum*  
503 *models of reinforced random walks*, Applied Mathematics Letters, 16 (2003), pp. 375–381.
- 504 [29] E. PALSSON AND H. G. OTHMER, *A model for individual and collective cell movement in*  
505 *dictyostelium discoideum*, Proceedings of the National Academy of Sciences, 97 (2000),  
506 pp. 10448–10453.
- 507 [30] J. K. PARRISH AND W. M. HAMNER, *Animal groups in three dimensions: how species aggregate*,  
508 Cambridge University Press, 1997.
- 509 [31] J. R. POTTS AND M. A. LEWIS, *Spatial memory and taxis-driven pattern formation in model*

- 510 *ecosystems*, Bulletin of Mathematical Biology, 81 (2019), pp. 2725–2747, [https://doi.org/](https://doi.org/10.1007/s11538-019-00626-9)  
511 [10.1007/s11538-019-00626-9](https://doi.org/10.1007/s11538-019-00626-9), <https://doi.org/10.1007/s11538-019-00626-9>.
- 512 [32] C. R. REID AND T. LATTY, *Collective behaviour and swarm intelligence in slime moulds*, FEMS  
513 Microbiology Reviews, 40 (2016), pp. 798–806.
- 514 [33] C. M. TOPAZ, A. L. BERTOZZI, AND M. A. LEWIS, *A nonlocal continuum model for biological*  
515 *aggregation*, Bulletin of Mathematical Biology, 68 (2006), p. 1601.
- 516 [34] P. TURCHIN, *Population consequences of aggregative movement*, Journal of Animal Ecology,  
517 (1989), pp. 75–100.
- 518 [35] P. A. WESTLEY, A. M. BERDAHL, C. J. TORNEY, AND D. BIRO, *Collective movement in ecology:*  
519 *from emerging technologies to conservation and management*, Phil. Trans. R. Soc. B, 373  
520 (2018), p. 20170004.
- 521 [36] J. YUAN, Y. ZHENG, AND X. XIE, *Discovering regions of different functions in a city using hu-*  
522 *man mobility and pois*, in Proceedings of the 18th ACM SIGKDD international conference  
523 on Knowledge discovery and data mining, 2012, pp. 186–194.